Journal of Applied Physics

RESEARCH ARTICLE | AUGUST 28 2024

Reproduction of single-to-double hysteresis transition of nuclear spin polarization in a single InAlAs quantum dot

Z.-R. Li; S. Yamamoto; S. Adachi; R. Kaji

J. Appl. Phys. 136, 084308 (2024)
https://doi.org/10.1063/5.0223272

Journal of Applied Physics | ARTICLE | pubs.aip.org/aip/jap

Reproduction of single-to-double hysteresis transition of nuclear spin polarization in a single InAlAs quantum dot

Cite as: J. Appl. Phys. **136**, 084308 (2024); doi: 10.1063/5.0223272
Submitted: 13 June 2024 · Accepted: 13 August 2024 ·
Published Online: 28 August 2024

View Online Export Citation CrossMark

Z.-R. Li,[1] S. Yamamoto,[2] S. Adachi,[1,a)] and R. Kaji[1,b)]

AFFILIATIONS

[1]Graduate School of Engineering, Hokkaido University, N13 W8, Kitaku, Sapporo 060-8628, Japan
[2]Department of Materials Science, Tohoku University, 6-6-02, Aramaki-aza Aoba, Aoba-ku, Sendai 980-8579, Japan

[a)]**Electronic mail:** adachi-s@eng.hokudai.ac.jp
[b)]**Author to whom correspondence should be addressed:** r-kaji@eng.hokudai.ac.jp

ABSTRACT

We have observed a transition from single to double hysteresis of nuclear spin polarization (NSP) with increasing magnetic field in a single InAlAs self-assembled quantum dot, which means the birth of a third stable branch that depends on the field strength. This NSP transition behavior could not be reproduced by standard model calculations using a fixed electron–nuclear spin correlation time τ_c under different external field conditions. By introducing the field dependence of τ_c, we were able to successfully reproduce the observed NSP transition. This finding on the phenomenological description of the magnetic field dependence will be a future highlight of τ_c.

I. INTRODUCTION

In semiconductor quantum dots (QDs), long carrier spin lifetime is realized by suppressing the translational motion,[1] while the influence of Fermi's contact hyperfine interaction (HFI) is highly enhanced due to strong localization of electron wavefunction. When a well-orientated electron spin is injected into a QD through optical selection rules,[2,3] the spin angular momentum is transferred easily from the electron to the lattice nuclear spin ensemble through the spin flip-flop process via the HFI.[4,5] The resultant nuclear spin polarization (NSP) $\langle I_z \rangle$ reacts on the spin-unpaired electrons in the form of an effective nuclear magnetic field (Overhauser field), $\boldsymbol{B}_n$, and can be detected macroscopically as the spectral energy shift of the electronic levels (Overhauser shift: OS).[6–8] Such an Overhauser field would prolong the electron spin coherence time,[9] and this feature is expected to contribute to the progress in quantum memory[10,11] and quantum information processing.[12]

Recently, we have observed *double bistability of NSP* and predicted an interesting transition from bistability to tristability (tristable response) in QDs by tuning the correlation time τ_c of the hyperfine coupling between electron and nuclear spins.[13,14] In a standard spin relaxation theory, τ_c is the time scale in which the direction and magnitude of the effective magnetic field can be approximated as stationary for an electron spin in a QD.[1,4,5,15,16] With the introduction of τ_c, each Zeeman-split electron state has a spread of $\hbar/\tau_c$. The overlap of these two levels determines the allowable spin flip-flop rate by the HFI without violating energy conservation during the process. Although τ_c is basically determined by what interactions are responsible for the spin relaxation and is usually treated as a constant, it can be modified actually by the sample temperature in self-assembled (SA) QDs[17] and bias voltage in charge-tunable QDs.[18] The external magnetic field $\boldsymbol{B}_{ext}$ is one of the key parameters in the studies of QD-NSP, but it has not been clarified how τ_c is affected by $\boldsymbol{B}_{ext}$.

In this paper, we show that the number of hysteresis loops in the QD-NSP changes from single to double as B_{ext} increases (referred to as "single-to-double hysteresis transition"). Since model calculations with τ_c as a constant is difficult to explain this observation, the magnetic field dependence of τ_c is studied experimentally and numerically.

II. EXPERIMENTS

The sample was single $In_{0.75}Al_{0.25}As/Al_{0.3}Ga_{0.7}As$ SAQDs grown on an undoped (001)-GaAs substrate.[6,19] A continuous-wave Ti:sapphire laser with the wavelength of 730 nm (~1.6986 eV) was used to inject spin-polarized carriers into the wetting layer. As shown in Fig. 1(a), two rotating half-wave plates (HWPs) were used; HWP1, placed between a pair of linear polarizers (LPs), controls the excitation power P_{exc}, and HWP2 with a quarter-wave plate (QWP) controls the excitation polarization. The excitation light was focused on the QD sample by an objective lens (OL, ×20) along the sample growth axis (z-axis). Photoluminescence (PL) from individual QDs passed through the same OL and was detected by a spectrometer and a Si-charge-coupled device (CCD) camera. The QD sample was kept at 6 K throughout all measurements. A superconducting magnet generated a static magnetic field along the z-axis, B_z, up to 5 T. The PL energy can be determined with an accuracy of 5 μeV by spectral fittings.

Figure 1(b) shows typical PL spectra of a single InAlAs SAQD at 0 T. In the following, only PL spectra from the ground state of the positive trion X^+ consisting of an electron and spin-singlet holes are discussed. For X^+ PL, the degree of circular polarization (DCP, ρ_c) is determined solely by the electron spin polarization, $\langle S_z \rangle$, with the relation $\langle S_z \rangle = \rho_c/2$. Here, ρ_c is defined as $\rho_c \equiv (I^- - I^+)/(I^- + I^+)$, where $I^\pm$ is the $\sigma^\pm$ polarized PL intensity.

Typical magneto-PL spectra of X^+ are shown in Fig. 1(c). The energy splitting of X^+ PL can be written as $\Delta E_Z = g_h \mu_B B_z + g_e \mu_B (B_z + B_{n,z}^{\text{stat}})$, where g_e (g_h) denotes the electron (hole) g-factor and μ_B is the Bohr magneton.[20,21] The second term on the right-hand side is the electronic Zeeman splitting and

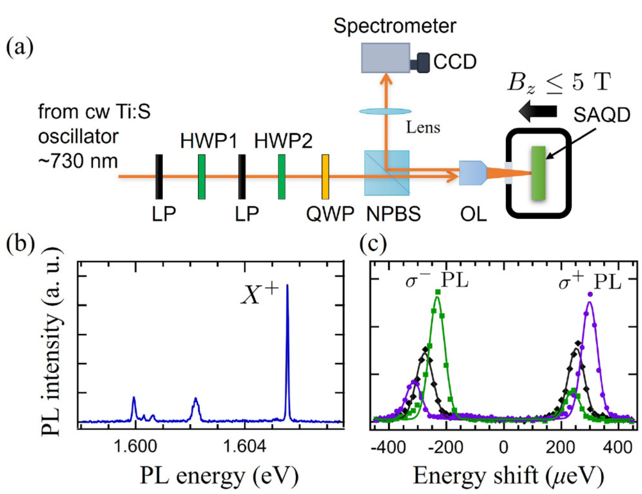

FIG. 1. (a) Schematics of the experimental apparatus in Faraday geometry. NPBS: non-polarizing beam splitter. (b) PL spectra from a target single QD at 0 T. (c) X^+ PL spectra at 4.0 T under linearly (π^x: diamonds) and circularly (σ^+/σ^-: circles/squares) polarized excitations with $P_{\text{exc}} = 370\,\mu$W. The solid lines are the fitting curves. Under $\sigma^{+(-)}$ excitation, $B_{n,z}^{\text{stat}}$ is aligned antiparallel (parallel) to $B_z > 0$, and thus, ΔE_Z increases (decreases) in our InAlAs QDs.

is affected by $B_{n,z}^{\text{stat}}$, the z-component of the static part of $\boldsymbol{B}_n$. OS is defined as $\Delta_{\text{OS}} \equiv 2\tilde{A}\langle I_z \rangle = g_e \mu_B B_{n,z}^{\text{stat}}$ ($\tilde{A}$: averaged HFI constant) and is the difference between ΔE_Z under circularly (σ^+/σ^-) and linearly (π^x) polarized excitations. In Fig. 1(c), Δ_{OS} was evaluated to be −86 (+53) μeV under σ^+ (σ^-) excitation at $B_z = 4.0$ T, where the optically generated $B_{n,z}^{\text{stat}}$ aligned antiparallel (parallel) to $B_z > 0$. In $In_{0.75}Al_{0.25}As$ SAQDs, the observed value of $|\Delta E_Z|$ increases (decreases) by Δ_{OS} under σ^+ (σ^-) excitation due to the relation $g_e \cdot g_h < 0$.[22]

III. RESULTS AND DISCUSSION

A. Transition from single to double hysteresis

Figures 2(a) and 2(b) summarize P_{exc}-dependences of Δ_{OS} and ρ_c under σ^+ excitation at various B_z, respectively. Solid and open circles (squares) are the observed Δ_{OS} (ρ_c) with increasing and decreasing P_{exc}, respectively. Within the range of P_{exc} used here, the fraction of time in which a QD is occupied with an electron

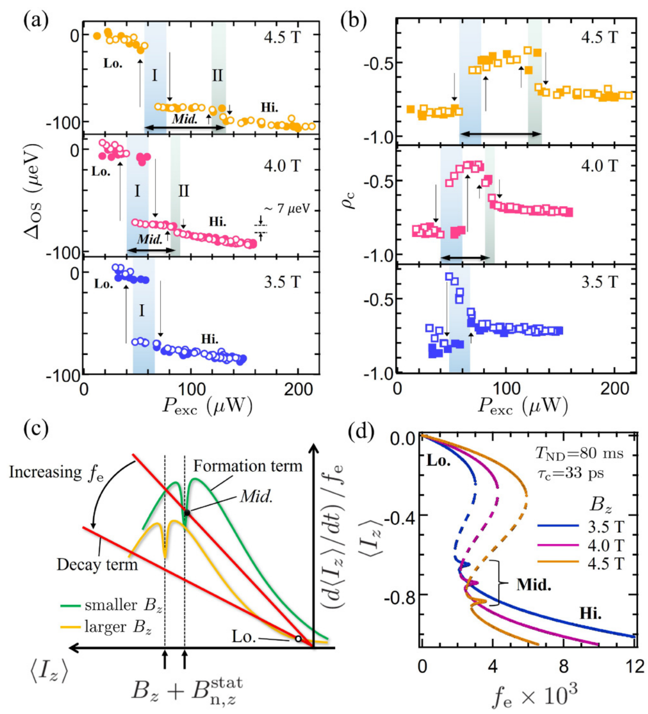

FIG. 2. P_{exc}-dependences of Δ_{OS} (a) and ρ_c (b) under σ^+ excitation at 3.5 (bottom), 4.0 (middle), and 4.5 T (top). Solid (open) markers are the observed values with increasing (decreasing) P_{exc}. (c) Schematics of the NSP formation (green, orange curves) and decay terms (red lines) as a function of $\langle I_z \rangle$. The dotted lines mark the field compensation points. The increase in f_e ($\propto P_{\text{exc}}$) reduces the slope of the decay term of NSP in this plot. (d) Calculations of $\langle I_z \rangle$ as a function of f_e at various B_z. The used parameters are $B_f = 40$ mT, $g_e = 0.32$, $\tau_c = 33$ ps, and $T_{\text{ND}} = 80$ ms, and all of them are assumed to be constant here. The dashed part indicates the unstable branch, and the narrow horizontal peaks correspond to the Mid. branch of NSP.

(denoted as f_e), is proportional to P_{exc} for $B_z \leq 4.0$ T. The saturation of the PL intensity appears for $P_{exc} > 200\,\mu$W at 4.5 T.

At $B_z = 3.5$ T, a unique hysteresis loop (I) appears as shown in the bottom panel of Fig. 2(a). As indicated by arrows, this loop connects two stable branches of NSP (Lo. and Hi.) at two points with abrupt jumps. Furthermore, the abrupt changes in ρ_c synchronized with Δ_{OS} were observed as shown in Fig. 2(b). These behaviors are characteristic of the bistability of NSP,[8,23,24] but changing B_z alters this well-known phenomenon; as B_z increases from 3.5 to 4.0 T [the middle panels], another hysteresis loop (II) appears in the higher P_{exc} region. This *double bistability* signifies the emergence of the third stable branch of NSP (Mid.).[13] Further increasing B_z up to 4.5 T, Mid. branch, the region between loop-I and loop-II, was extended as shown in the top panels. This is *single-to-double hysteresis transition*, and a similar trend has been reported in our previous study.[13]

Note that the Mid. branch located between Hi. and Lo. branches is more clearly identified by the change in $|\rho_c|$ than the one in $|\Delta_{OS}|$. While there is an obvious correlation between ρ_c ($\propto\langle S_z\rangle$) and Δ_{OS} ($\propto\langle I_z\rangle$) as shown later, the fact that $|\rho_c|$ is quite sensitive to the small change in Δ_{OS} comparable to the energy resolution in our measurement system is a great help in detecting the Mid. branch.

Figure 2(c) illustrates how the experimentally observed NSP branch evolves as P_{exc} and B_{ext} are varied. Lorentzian curves with a sharp dip (green, orange) and red straight lines represent the formation and decay terms of NSP. The phenomenological model for the electron–nuclear spin system and the explicit form of the formation term are seen in the Appendix. The steady state of $\langle I_z\rangle$ corresponding to the observed value is depicted as the intersection of the formation and decay terms. The height of the formation term ($1/T_{NF}$) increases linearly with increasing f_e ($\propto P_{exc}$). On the other hand, the slope of the decay term, which is given by the inverse of the decay time T_{ND} of NSP, is invariant to changes in f_e. When the formation term is normalized to fix its height in the plot, an increase in f_e leads to a decrease in the slope of the decay term. As f_e changes, the intersection undergoes abrupt transition so that the observed NSP jumps to a different branch accordingly.

It should be noted that the origin of the Mid. branch is the nuclear spin fluctuations (NSFs). The NSP consists of the following two parts: a stationary part, which is responsible for $B_{n,z}^{stat}$ and a temporally fluctuating part. The latter one, NSF, causes a sharp reduction in $|\langle S_z\rangle|$ resulting in a dip structure of the NSP formation term at the field compensation point $B_z + B_{n,z}^{stat} = 0$. The magnitude of NSF, which is reduced to the effective magnetic field B_f, has been evaluated as $\sim$40 mT experimentally in our InAlAs QDs.[22] The depth and width of the dip are essentially determined by B_f, and we found that a large B_f is suitable for the Mid. branch observation.[13]

Figure 2(d) shows the calculated results of NSP as a function of f_e. The key parameters here are $B_f = 40$ mT, $g_e = 0.32$, $\tau_c = 33$ ps, and $T_{ND} = 80$ ms; the latter three were determined from fitting of data set similar to Fig. 4(b) (but obtained at 3.5 T). In this figure, these parameters were assumed to be independent not only of f_e but also of B_z. Considering the impact of NSF, a narrow horizontal peak corresponding to the Mid. branch appears within the *S*-shaped hysteresis loop. For the Mid. branch to be observed, the tip of this narrow peak must grow to f_e larger than f_e at the end of the Lo. branch, otherwise only the transition between Lo. and Hi. branches can be observed. However, the calculations show that as B_z is increased, the length of the Mid. branch remains almost the same, but the width of the outer *S*-shaped loop increases. Therefore, this model indicates that the Mid. branch is less likely to be observed with increasing B_z. This is not consistent with the experimental results shown in Figs. 2(a) and 2(b).

Here, we consider the effects of increasing B_z on the trajectory of the intersection [Fig. 2(c)]. Note that the observability of the Mid. branch depends on the ease of transition from the Lo. (or Hi.) branch and whether there is an intersection in the dip region of the formation term. These factors depend on the dip depth and the gradient of $1/T_{NF}$ around the transition point (especially from Lo.). As B_z increases, the height of the formation term is reduced and the peak position shifts toward the higher $\langle I_z\rangle$ side. In this change, while the dip depth remains almost the same, the gradient of $1/T_{NF}$ at the lower transition point (open circle) becomes more gradual. Thus, the NSP at the Lo. branch tends to stay in the original Lo. branch, even if f_e increases (called *Lo.-restraint*). To get out from the Lo. branch, the slope of the decay term needs to be much smaller (i.e., larger value of f_e), but this would make it harder to get the intersection in the dip region. As a result, the transition between Lo. and Hi. branches is more likely to occur at higher B_z, making it difficult to access the Mid. branch in this model.

To reproduce the single-to-double hysteresis transition, we introduce B_z-dependence to the parameters that have been treated as constants. Although multiple parameters affect the NSP intricately, only the following three seem to depend on B_z: T_{ND}, B_f, and τ_c.[25]

First, we consider the B_z-dependence of T_{ND}. It has been reported that T_{ND} is actually prolonged with increasing B_z.[26,27] This is because an additional NSP-decay process, which is activated by the nuclear quadrupole interaction, is effectively suppressed by increasing B_z. However, model calculations in Fig. 3(a) show that the longer T_{ND} shortens the length of the Mid. branch and makes it difficult to access. Furthermore, the prolongation of T_{ND} appears

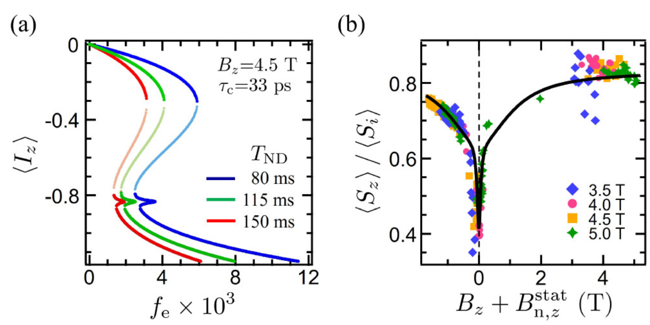

FIG. 3. (a) Calculated f_e-dependencies of $\langle I_z\rangle$ with various T_{ND}. (b) Experimentally obtained $\langle S_z\rangle$ as a function of $B_z + B_{n,z}^{stat}$. The vertical axis is normalized by $\langle S_i\rangle$, the initial value of electron spin polarization. The absence of data points around $B_z + B_{n,z}^{stat} = 0.3 \sim 3.0$ T is due to the abrupt change of NSP. The solid curve is the theoretical one using Eq. (A5).

only in the sub-Tesla region,[27] and $T_{\rm ND}$ can be treated as a constant under the high-B_z conditions currently considered. Therefore, it can be reasonably assumed that the change in $T_{\rm ND}$ does not play a significant role in the single-to-double hysteresis transition.

Next, we consider the possibility that $B_{\rm f}$ varies depending on B_z. In previous works,[1,8,24,28] $B_{\rm f}$ has been given by $B_{\rm f} \sim \tilde{A}\tilde{I}/(g_e\mu_B\sqrt{N})$ ($\tilde{I}$ is the averaged nuclear spin and N is the number of nuclei in the localization volume of the electron) and considered to be independent of B_z. Figure 3(b) supports this independence of B_z. The figure shows the experimentally deduced $\langle S_z\rangle$ as a function of the total magnetic field ($= B_z + B^{\rm stat}_{{\rm n},z}$) seen by an electron, where the data set was obtained at several B_z from 3.5 to 5.0 T. As clearly shown, a sharp reduction of $\langle S_z\rangle$ occurs at $B_z + B^{\rm stat}_{{\rm n},z} = 0$, where only $B_{\rm f}$ affects on $\langle S_z\rangle$. The data points under all B_z are distributed around a single calculated curve, which strongly suggests that $B_{\rm f}$, which determines the shape of the curve, is independent of B_z. Furthermore, no clear difference in $B_{\rm f}$ deduced from the data for each B_z was found. This is consistent with the previous work.[13]

B. Magnetic field dependence of τ_c

From the above discussion, we considered it most likely that τ_c has the magnetic field dependence. To examine this assumption, we focused on the excitation polarization dependencies of $\langle S_z\rangle$ and $\langle I_z\rangle$ at various B_z. Figure 4(a) summarizes the deduced $\langle I_z\rangle$ and $\langle S_z\rangle$ as a function of the excitation light polarization $\rho_c^{\rm exc}$ at $B_z = 4.2$ T. The horizontal axis was normalized by $\rho^{\rm exc}_{\rm c,\,max}$, the maximum value of $|\rho_c^{\rm exc}|$, and $\rho_c^{\rm exc}/\rho^{\rm exc}_{\rm c,\,max} = +1\ (-1)$ corresponds to the case under σ^- (σ^+) excitation. When $B^{\rm stat}_{{\rm n},z}$ is oriented opposite to B_z at $\rho_c^{\rm exc} < 0$, the double bistability of NSP clearly appears with respect to the change in $\rho_c^{\rm exc}$. On the other hand, $\langle I_z\rangle$ and $\langle S_z\rangle$ show monotonic changes when $B^{\rm stat}_{{\rm n},z}$ is parallel to B_z at $\rho_c^{\rm exc} > 0$. From the data set in Fig. 4(a), the correlation between $\langle I_z\rangle$ and $\langle S_z\rangle$ can be plotted as shown in Fig. 4(b). Due to the transition between Hi. and Mid. branches, no data points appear in the region between $\langle S_z\rangle$ of -0.3 and -0.2. On the other hand, an abrupt change in $\langle I_z\rangle$ is observed at $\langle S_z\rangle \sim -0.2$, which corresponds to the transition between Mid. and Lo. branches.

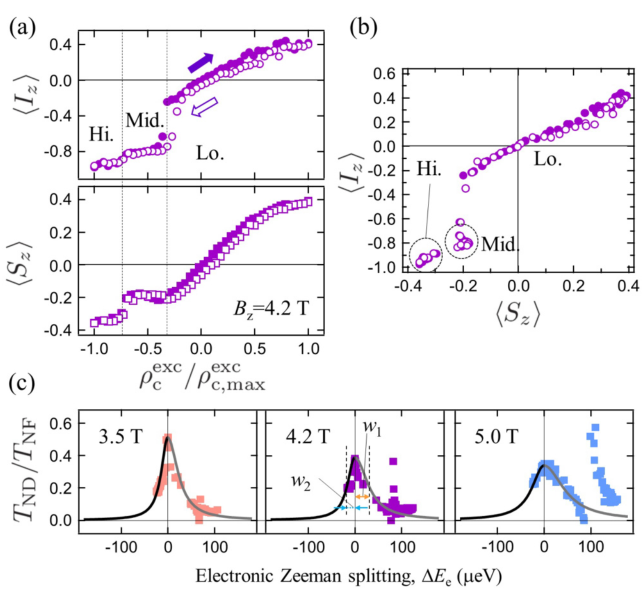

FIG. 4. (a) Excitation polarization dependence on $\langle I_z\rangle$ (upper panel) and $\langle S_z\rangle$ (lower panel) at $B_z = 4.2$ T, while keeping $P_{\rm exc}$ fixed. The horizontal axis is the normalized DCP of excitation light. The solid (open) markers indicate the values with increasing (decreasing) $\rho_c^{\rm exc}$. (b) Correlation between $\langle I_z\rangle$ and $\langle S_z\rangle$ at 4.2 T, where data points are from (a). (c) The deduced $T_{\rm ND}/T_{\rm NF}$ as a function of ΔE_e at 3.5 (left), 4.2 (center), and 5.0 T (right). Black (gray) curves are the fittings on negative (positive) ΔE_e.

By assuming that the electron spin polarization at thermal equilibrium is negligible, the steady-state condition of NSP leads to the following relation [see Eqs. (A1) and (A2) in the Appendix]:

$$\frac{T_{\rm ND}}{T_{\rm NF}} = \frac{\langle I_z\rangle}{Q\langle S_z\rangle - \langle I_z\rangle} \propto \frac{1/\tau_c}{(\hbar/\tau_c)^2 + \Delta E_e^2}, \tag{1}$$

where Q is a spin conversion coefficient from electron to nucleus and is $\sim$16.33 in our InAlAs QDs. This formula suggests that the ratio of $T_{\rm ND}$ to $T_{\rm NF}$ can be evaluated using a set of $\langle I_z\rangle$ and $\langle S_z\rangle$ and that it draws a Lorentzian shape with respect to the electronic Zeeman splitting, ΔE_e. The most important point is that $1/\tau_c$ is reflected as the half width of the Lorentzian curve.

Figure 4(c) shows the deduced $T_{\rm ND}/T_{\rm NF}$ as a function of ΔE_e at three different B_z: 3.5 (left), 4.2 (middle), and 5.0 T (right). For all B_z, the deduced $T_{\rm ND}/T_{\rm NF}$ has a peak structure centered at $\Delta E_e = 0$. As B_z increases, the peak width increases, while its height decreases. According to Eq. (1), these changes in the peak shape should reflect the B_z-dependence of τ_c. The spike structure appears in $\Delta E_e > 0$, which is pronounced at 4.2 and 5.0 T, is considered an artifact. This spike consists of data when the excitation polarization is close to linear (i.e., $\langle S_z\rangle \sim 0$), and thus, the denominator of Eq. (1) is close to zero around this point, leading to an unintended magnification of the measured values.

The curves in Fig. 4(c) were asymmetric with respect to ΔE_e, contrary to expectations. However, we attempted to evaluate the curve width by dividing the data into two intervals and fitting to each; w_1 (w_2) is the half width of the Lorentzian curve in the region of $\Delta E_e > 0$ ($\Delta E_e < 0$). Note that τ_c and $T_{\rm ND}$ were used as variable parameters in the fittings.

Figure 5(a) summarizes the deduced w_1 and w_2 (orange and blue solid circles) as a function of B_z. Both w_1 and w_2 monotonically increase with increasing B_z, and similar trend has been observed in other single QDs (open circles). Since the peak width is proportional to $1/\tau_c$ from Eq. (1), we estimated the corresponding τ_c values, i.e., τ_{c1} from w_1 and τ_{c2} from w_2. Figure 5(b) summarizes the deduced τ_c as a function of B_z. In the present analysis, two τ_c values were deduced for each B_z, but both τ_{c1} and τ_{c2} show the same trend and decrease with increasing B_z.

Note that the experimentally obtained τ_c in our InAlAs QDs is on the order of a few 10 ps in the range of B_z up to 5 T. This is the same order of magnitude as reported in InGaAs QDs.[17] It is not clear which process is most related to the microscopic origin of τ_c in this study. This is because any process which limits the

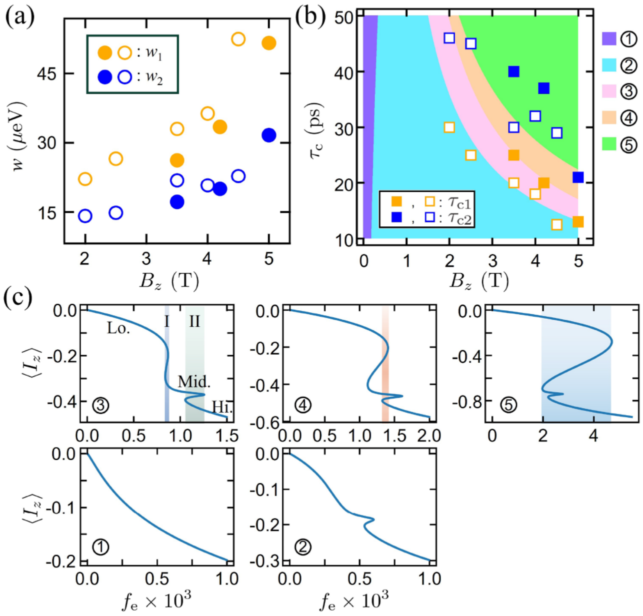

FIG. 5. (a) and (b) Peak widths (w_1, w_2) and the corresponding correlation time (τ_{c1}, τ_{c2}) as a function of B_z. The solid markers were deduced from Fig. 4(c), and the open markers were obtained from other single InAlAs QD with the same procedure. In addition, the computed diagram of τ_c and B_z was superimposed so that it can be compared with the experimental data. (c) Typical f_e-dependence of $\langle I_z \rangle$ in each zone of (b). Double bistability and tristability appear only in the narrow area of zone 3 and zone 4, respectively.

interaction time between the spin-polarized electron and the nuclei will affect τ_c. Currently, we consider that the energy relaxation following non-resonant optical excitation has the largest impact on τ_c under our experimental conditions.[29]

The computed diagram of τ_c and B_z is overlaid in Fig. 5(b) for comparison with the observed results. This diagram is divided into five zones depending on the combination of τ_c and B_z, and it clearly shows how the change in τ_c is involved in the single-to-double hysteresis transition observed when B_z is varied. The typical f_e-dependence of $\langle I_z \rangle$ in each zone is summarized in Fig. 5(c).

In zone 1, where B_z is small, $|\langle I_z \rangle|$ changes monotonically with f_e regardless of τ_c. The monotonicity of $\langle I_z \rangle$ remains in zone 2, but a horizontal dip structure appears. This is because the field compensation point begins to appear from this zone. Above zone 3, hysteresis loops of $\langle I_z \rangle$ appear. In zone 3, $\langle I_z \rangle$ shows the double bistability, i.e., loop-I and loop-II occur in different f_e regions. In zone 4, we can see the tristability with three stable branches (and two unstable branches) for one f_e. In zone 5 with larger B_z and longer τ_c, the typical bistability with loop-I only appears because the width of the hysteresis loop exceeds the length of the Mid.branch. Interestingly, only in a small area (zones 3 and 4), the phenomena associated with the Mid.branch emerge. The transition from zone 5 to zone 3 corresponds to the experimentally observed single-to-double transition [Fig. 2(a)]. From the diagram, the transition from zone 5 to zone 3 with increasing B_z requires a shortening of τ_c. This behavior agrees with the experimentally observed B_z-dependence of τ_c, and it strongly supports our scenario that τ_c depends on the magnetic field.

Finally, we note that our findings are not limited to any particular material or structure. The key ingredient for the appearance of double bistability is the NSF, known as the source of localized electron spin relaxation in many materials with nonzero nuclear spin (e.g., In(Ga)As, ZnO,[30] and InP[31]). It is, therefore, likely that similar phenomena occur in any QD as long as the HFI works. The electrically controllable QDs, such as self-assembled QDs embedded in diode structures or gate-defined QDs, may help to further elucidate the physics through its potential controllability of τ_c.[18]

IV. CONCLUSIONS

We have demonstrated that the correlation time of the hyperfine coupling τ_c varies with the external magnetic field, taking the observed single-to-double hysteresis transition of the nuclear spin polarization as a clue. τ_c was evaluated experimentally based on the standard model equation and found to shorten with an increasing external magnetic field. This concept of the magnetic field dependence of τ_c successfully reproduced the recently discovered phenomenon of *double bistability*. The single-to-double hysteresis transition of the nuclear spin polarization has potential for realizing physical reservoir computing,[32] where the system with nonlinear response to the input and short-term memory for the state is required. Our findings indicate that the nonlinearity of electron and nuclear spin-coupled system mediated by the hyperfine interaction can be tuned by controlling τ_c.

τ_c is an important parameter in describing the electron–nuclear spin-coupled system. However, there have been few reports focusing on τ_c itself and much remains to be clarified. Our findings shed light on τ_c and its controllability, providing not only a tuning knob but useful information for future quantum state control in the electron–nuclear spin-coupled system.

ACKNOWLEDGMENTS

This work was supported by the Japan Society for the Promotion of Science (JSPS) KAKENHI Grant Nos. JP21H01745 and JP24K08189. This work was partially supported by a research grant from The Mazda Foundation.

AUTHOR DECLARATIONS

Conflict of Interest

The authors have no conflicts to disclose.

Author Contributions

Z.-R. Li: Data curation (lead); Formal analysis (lead); Investigation (lead); Visualization (lead); Writing – original draft (equal). **S. Yamamoto:** Formal analysis (equal); Investigation (equal); Software (equal); Visualization (equal); Writing – review & editing (equal). **S. Adachi:** Funding acquisition (equal); Investigation (equal); Supervision (lead); Writing – original draft (equal);

Writing – review & editing (equal). **R. Kaji:** Conceptualization (equal); Funding acquisition (equal); Investigation (equal); Methodology (equal); Project administration (equal); Supervision (equal); Writing – original draft (equal); Writing – review & editing (lead).

DATA AVAILABILITY

The data that support the findings of this study are available from the corresponding author upon reasonable request.

APPENDIX: PHYSICAL MODEL OF ELECTRON–NUCLEAR SPIN DYNAMICS

In general, the temporal evolution of $\langle I_z\rangle$ has been expressed in the following phenomenological form:[24]

$$\frac{d\langle I_z\rangle}{dt} = \frac{1}{T_{\rm NF}}\left[Q(\langle S_z\rangle - \langle S_z^{\rm eq}\rangle) - \langle I_z\rangle\right] - \frac{1}{T_{\rm ND}}\langle I_z\rangle, \quad \text{(A1)}$$

where $\langle S_z^{\rm eq}\rangle$ is the electron spin polarization at thermal equilibrium. The NSP formation rate, $1/T_{\rm NF}$, is given by

$$\frac{1}{T_{\rm NF}} = \frac{2f_{\rm e}\tau_{\rm c}(\tilde{A}/N)^2}{\hbar^2 + [g_{\rm e}\mu_{\rm B}(B_z + B_{{\rm n},z}^{\rm stat})\tau_{\rm c}]^2}. \quad \text{(A2)}$$

Since the electron spin-flip relaxation with a characteristic time of $\tau_{\rm hf}$ originates from the HFI, $1/\tau_{\rm hf}$ is proportional to the NSP formation rate[13,14,33]

$$\frac{1}{\tau_{\rm hf}} = \frac{NQ}{f_{\rm e}}\frac{1}{T_{\rm NF}}. \quad \text{(A3)}$$

The effect of nuclear field $\boldsymbol{B}_{\rm n}$ on the electron spin can be seen as *frozen*,[33] and we separated $\boldsymbol{B}_{\rm n}$ into a stationary part $\boldsymbol{B}_{\rm n}^{\rm stat}$ and a fluctuating part $\boldsymbol{B}_{\rm f}$. The Bloch equation expresses the dynamics of electron spin $\boldsymbol{S}$ as

$$\frac{d\boldsymbol{S}}{dt} = \frac{g_{\rm e}\mu_{\rm B}(\boldsymbol{B}_{\rm ext} + \boldsymbol{B}_{\rm n})}{\hbar}\times\boldsymbol{S} - \frac{1}{\tau_{\rm r}}(\boldsymbol{S} - \boldsymbol{S}_{\rm i}) - \left(\frac{1}{\tau_{\rm s}^{\rm int}} + \frac{1}{\tau_{\rm hf}}\right)\boldsymbol{S}, \quad \text{(A4)}$$

where $\boldsymbol{S}_{\rm i}$ is the initial electron spin, $\tau_{\rm r}$ is the recombination time, and $\tau_{\rm s}^{\rm int}$ is the spin relaxation time excluding the effect of HFI. The steady-state solution of Eq. (A4) yields $\langle S_z\rangle$ in the following equation:

$$\langle S_z\rangle = \left(\frac{\tau_{\rm e}}{\tau_{\rm r}}\right)\langle S_{\rm i}\rangle\frac{B_{1/2}^2 + \langle B_{{\rm f},z}^2\rangle + \left(B_z + B_{{\rm n},z}^{\rm stat}\right)^2}{B_{1/2}^2 + \langle B_{\rm f}^2\rangle + \left(B_z + B_{{\rm n},z}^{\rm stat}\right)^2}. \quad \text{(A5)}$$

Here, $B_{1/2} = \hbar/(g_{\rm e}\mu_{\rm B}\tau_{\rm e})$ is the reduced value of the electron spin lifetime, $\tau_{\rm e}$, given by $\tau_{\rm e} = 1/(1/\tau_{\rm r} + 1/\tau_{\rm s}^{\rm int} + 1/\tau_{\rm hf})$. The spatial distribution of $B_{\rm f}$ is assumed to be isotropic $\langle B_{\rm f}^2\rangle = 3\langle B_{{\rm f},z}^2\rangle$.[34]

REFERENCES

[1] I. A. Merkulov, A. L. Efros, and M. Rosen, Phys. Rev. B **65**, 205309 (2002).

[2] S. Cortez, O. Krebs, S. Laurent, M. Senes, X. Marie, P. Voisin, R. Ferreira, G. Bastard, J. M. Gerard, and T. Amand, Phys. Rev. Lett. **89**, 207401 (2002).

[3] G. Lampel, Phys. Rev. Lett. **20**, 491 (1968).

[4] M. I. Dyakonov and V. I. Perel, in *Optical Orientation*, Modern Problems in Condensed Matter Sciences, edited by F. Meier and B. Zakharchenya (North-Holland, Amsterdam, 1984), Vol. 8, Chap. 2.

[5] V. G. Fleisher and I. A. Merkulov, in *Optical Orientation*, Modern Problems in Condensed Matter Sciences, edited by F. Meier and B. Zakharchenya (North-Holland, Amsterdam, 1984), Vol. 8, Chap. 5.

[6] T. Yokoi, S. Adachi, H. Sasakura, S. Muto, H. Z. Song, T. Usuki, and S. Hirose, Phys. Rev. B **71**, 041307(R) (2005).

[7] P. Maletinsky, C. W. Lai, A. Badolato, and A. Imamoglu, Phys. Rev. B **75**, 035409 (2007).

[8] R. Kaji, S. Adachi, H. Sasakura, and S. Muto, Phys. Rev. B **77**, 115345 (2008).

[9] C. Latta, A. Srivastava, and A. Imamoğlu, Phys. Rev. Lett. **107**, 167401 (2011).

[10] E. V. Denning, D. A. Gangloff, M. Atatüre, J. Mørk, and C. L. Gall, Phys. Rev. Lett. **123**, 140502 (2019).

[11] J. M. Taylor, C. M. Marcus, and M. D. Lukin, Phys. Rev. Lett. **90**, 206803 (2003).

[12] D. D. Awschalom, D. Loss, and N. Samarth, *Semiconductor Spintronics and Quantum Computing* (Springer-Verlag, Berlin, 2002).

[13] S. Yamamoto, R. Kaji, H. Sasakura, and S. Adachi, Phys. Rev. B **101**, 245424 (2020).

[14] S. Yamamoto, R. Kaji, H. Sasakura, and S. Adachi, JJAP **60**, SBBH07 (2021).

[15] M. I. Dyakonov, in *Spin Physics in Semiconductors*, Springer Series in Solid-State Sciences, edited by M. I. Dyakonov (Springer, Berlin, 2008), Vol. 157, Chap. 1.

[16] V. K. Kalevic, K. V. Kavokin, and I. A. Merkulov, in *Spin Physics in Semiconductors*, Springer Series in Solid-State Sciences, edited by M. I. Dyakonov (Springer, Berlin, 2008), Vol. 157, Chap. 11.

[17] B. Urbaszek, P.-F. Braun, T. Amand, O. Krebs, T. Belhadj, A. Lemaítre, P. Voisin, and X. Marie, Phys. Rev. B **76**, 201301(R) (2007).

[18] J. Nilsson, L. Bouet, A. J. Bennett, T. Amand, R. M. Stevenson, I. Farrer, D. A. Ritchie, S. Kunz, X. Marie, A. J. Shields, and B. Urbaszek, Phys. Rev. B **88**, 085306 (2013).

[19] H. Sasakura, S. Adachi, S. Muto, H. Z. Song, T. Miyazawa, and Y. Nakata, Phys. E **21**, 511 (2004).

[20] Note that the influence of $\boldsymbol{B}_{\rm n}$ on the hole spin can be safely ignored. This is because the probability of a hole spin at a nuclear site and the resulting coupling constant of the HFI are quite small.

[21] B. Eble, C. Testelin, P. Desfonds, F. Bernardot, A. Balocchi, T. Amand, A. Miard, A. Lemaître, X. Marie, and M. Chamarro, Phys. Rev. Lett. **102**, 146601 (2009).

[22] R. Kaji, S. Adachi, H. Sasakura, and S. Muto, Phys. Rev. B **85**, 155315 (2012).

[23] A. I. Tartakovskii, T. Wright, A. Russell, V. I. Falko, A. B. Van'kov, J. Skiba-Szymanska, I. Drouzas, R. S. Kolodka, M. S. Skolnick, P. W. Fry, A. Tahraoui, H.-Y. Liu, and M. Hopkinson, Phys. Rev. Lett. **98**, 026806 (2007).

[24] B. Urbaszek, X. Marie, T. Amand, O. Krebs, P. Voisin, P. Maletinsky, A. Högele, and A. Imamoglu, Rev. Mod. Phys. **85**, 79-133 (2013).

[25] Other parameters such as $\tilde{A}$ and N are basically determined by the material and size of a target QD, and thus, it is reasonable to assume that they are independent of experimental parameters like B_z.

[26] C.-W. Huang and X. Hu, Phys. Rev. B **81**, 205304 (2010).

[27] R. Matsusaki, R. Kaji, S. Yamamoto, H. Sasakura, and S. Adachi, Appl. Phys. Express **11**, 085201 (2018).

[28] R. Kaji, R. Matsusaki, S. Yamamoto, and S. Adachi, Jpn. J. Appl. **58**, SBBH05 (2019).

[29] In InAs QDs embedded in a GaAs diode structure, it has been reported that $\tau_{\rm c}$ can increase up to several hundred picoseconds depending on the gate voltage.[18] Their observation suggests that the carrier tunneling event has a large impact on $\tau_{\rm c}$ in charge-tunable devices. However, in our sample, this effect is negligible because the InAlAs QD layer is sandwiched with thick AlGaAs barrier layers.

[30]W. K. Liu, K. M. Whitaker, A. L. Smith, K. R. Kittilstved, B. H. Robinson, and D. R. Gamelin, Phys. Rev. Lett. **98**, 186804 (2007).
[31]Y. Masumoto, S. Oguchi, B. Pal, and M. Ikezawa, Phys. Rev. B **74**, 205332 (2006).
[32]K. Nakajima, Jpn. J. Appl. Phys. **59**, 060501 (2020).
[33]O. Krebs, B. Eble, A. Lemaître, P. Voisin, B. Urbaszek, T. Amand, and X. Marie, C. R. Physique **9**, 874 (2008).
[34]M. S. Kuznetsova, K. Flisinski, I. Y. Gerlovin, I. V. Ignatiev, K. V. Kavokin, S. Y. Verbin, D. R. Yakovlev, D. Reuter, A. D. Wieck, and M. Bayer, Phys. Rev. B **87**, 235320 (2013).